STANFORD RESEARCH INSTITUTE
MENLO PARK CALIFORNIA

April 1, 1962

Progress Report No. 20
For the period February 1 to March 31, 1962

TUNGSTEN AND ROCKET MOTORS

SRI Project No. PU-2785
Contract NOrd-18619

Prepared for:
Special Projects Office
Department of the Navy
Bureau of Naval Weapons
Washington 25, D. C.

Introduction

The present study deals with two significant problems encountered in the use of tungsten as a solid-propellant rocket nozzle material. The first problem, tungsten erosion, is being studied under simulated exhaust conditions by a specially constructed plasma torch apparatus. The second problem, thermal shock cracking under rapid heat-up conditions is being investigated and the experimental results will be correlated with a mathematical analysis.

Discussion

Erosion Study Employing Plasma-Jet Exhaust Simulator

Data was previously reported for two types of W eroded in a high velocity plasma containing CO_2. The maximum specimen temperature at the start of each run was between 3100 and 3200°C (5612-5792°F). These results, shown again in Fig. 1, are plotted as average mass erosion rate ($mg\text{-}sec^{-1}$) versus CO_2 flow-rate ($mg\text{-}sec^{-1}$) for both W + 2% Th and for fine grain, pressed, sintered, and swaged W (fg-pss W). The erosion rate results would be much more meaningful if they were expressed in units of mass x $time^{-1}$ x $area^{-1}$ (e.g., $mg\text{-}sec^{-1}\text{-}cm^{-2}$). The asymmetry of the erosion zone had appeared to prevent the use of such units, but further analysis indicates an approximate expression containing those units is possible. Results in these desirable erosion rate units are usually obtained by surface recession measurements. For small amounts of erosion the weight loss rate per unit area is related to the surface recession rate by the expression:

62-3-1

$$\frac{\dot{\Delta m}}{A} = \rho \dot{\Delta r} \qquad (1)$$

where

$\dot{\Delta m}$ = Mass erosion rate

$\dot{\Delta r}$ = Surface recession rate

A = Erosion surface area

ρ = Density

For the results reported in Fig. 1, the corresponding maximum surface recessions are appreciable (10 to 50 mils on specimen diameters of 90 to 94 mils). Further, the recession is not uniform around the specimen diameter but occurs almost entirely on the plasma impingement side of the specimen. Nevertheless, these measurements have the advantages that the maximum recession occurred where the maximum temperature was measured and that at least for very small recessions, equation (1) would be valid.

Consequently, during the current reporting period, the maximum decrease in specimen diameter (essentially equivalent to the decrease in radius on the plasma impingement side of the specimen) was measured for the specimens represented in Fig. 1. The results are plotted as the averaged maximum surface recession rate (mils sec^{-1}) versus CO_2 flow rate in Fig. 2. Comparison of Figs. 1 and 2 shows the same general shape and trends, although the apparent difference in erosion rates between fg-pss W and W + 2% Th becomes evident at somewhat lower flow rates in Fig. 1.

Figure 3 is a plot of the maximum surface recession rate measurements from Fig. 2 versus the average mass erosion rate data from Fig. 1. The resulting curve is approximately linear, even for the measurements taken at high CO_2 flow rates. From Fig. 3 and equation (1) we can calculate an "effective erosion surface area" and compare it with an erosion area calculated from geometrical considerations.

From equation (1) $\frac{\dot{\Delta r}}{\dot{\Delta m}} = \frac{1}{\rho A}$

and since Fig. 3 indicates that $\dot{\Delta r}$ versus $\dot{\Delta m}$ is approximately linear,

$$\frac{1}{\rho A} = \text{slope Fig. 3} = 6.55 \times 10^{-2} \text{ in. gm}^{-1}$$

Using $\rho = 19.3 \text{ gm/cm}^3 = 316 \text{ gm/in.}^3$

then $$A = \frac{1}{316 \times 6.55 \times 10^{-2}} = 4.84 \times 10^{-2} \text{ in.}^2 \qquad (2)$$

from experimentally determined data.

For comparison with equation (2) we can calculate the surface area from geometrical considerations as follows:

The area under consideration will most likely approximate a hemi-cylinder since the plasma impinges on one side only. Thus,

$$A = \pi r_o L_o \tag{3}$$

where

r_o = initial radius of specimen = .045 in. for fg-pss W

L_o = initial length of erosion zone.

For runs at relatively low CO_2 flow rates L_o was found to be approximately 5/16 in., which is also the approximate plasma diameter.

From equation (3)

$$A = (.045)(.313) = 4.42 \times 10^{-2} \text{ in.}^2 \tag{4}$$

which compares favorably with the area calculated by equation (2) from experimentally determined erosion data.

Thus the erosion rates in Figs. 1 and 2 can be converted to approximate units of mass x area^{-1} x time^{-1} by use of equation (1) for the surface recession rate results and equation (2) for the mass erosion rates. It is estimated that these conversions would be fairly good for CO_2 flow rates up to approximately 35 mg-sec^{-1} but that for higher flow rates the assumptions in deriving equation (1) are no longer valid. Further experiments are planned to determine the accuracy of these conversions.

Attempts were made to determine data similar to Figs. 1 and 2 but at lower starting temperatures. These experiments were made in a new Vycor chamber with a removable sight glass so that approximate temperatures during the run could be measured. To achieve these lower temperatures it was necessary to move the specimen downstream in the plasma. At moderate to high flow rates the CO_2 pinched down the plasma so much that it converged in front of the specimen. This caused the specimen to be cooled to a very low temperature, and caused the impinging CO_2 to be dispersed along the length of the specimen.

It was then decided that further runs would be made at a lower range of exhaust constituent flow rates.

Specimens of fg-pss W were run for sixty seconds at CO_2 flow rates of $13.0 \pm .5$ mg-sec^{-1} at various temperatures. The results of these experiments are shown in Fig. 4 which plots both the maximum surface recession rate and the mass erosion rate for each specimen versus the average specimen temperature during the run. Both measurements indicate that changes in reaction temperature in the range 2800 to 3350°C produce relatively small changes in erosion rate.

Comparing Fig. 4 with Figs. 1 and 2 indicates that, for the conditions studied, the erosion rate of W in CO_2 appears much less sensitive to temperature than to the quantity of CO_2 impinging on the specimen surface.

Thermal Shock Study

Work is continuing on the measurement and calculation of thermal stresses and strains occurring on the outside surface of hollow tungsten cylinders subjected to rapid heat-up conditions. Also, a mathematical analysis is being made of the thermal stresses in hollow cylinders (see Appendix).

Using previously described strain and temperature measuring equipment,[1] it is now possible to record simultaneously, axial strain and surface temperature of the W specimen during each thermal shock test run. By determining the total strain and outside surface temperature, it is then possible to calculate the thermal stress and corresponding thermal strain at the outside surface with only a minimum of material property data. In cases where it is experimentally unfeasible to measure this strain (e.g., an actual rocket firing), it is necessary to obtain the actual temperature distribution, and accurate values of thermal, mechanical, and elastic material properties over an extremely broad temperature range, in order to obtain an estimate of the stresses which cause thermal shock failures. This procedure is made very difficult by the extreme variation in material property data which is revealed by an examination of the literature.

An analysis of a thermal shock test run is presented below for a 94% dense, pressed, and sintered tungsten cylinder (0.75-in. high x 1.14-in. I.D. x 1.54-in. O.D.) in which a circumferential crack was located after the run.

Surface Heat-Up Data

A temperature versus time plot is shown for the "cold" outside surface of the cylinder in Fig. 5. During the three-second interval that the heater power remained on, the outside temperature rose from 70°F to about 1100°F. With the power off, the temperature continued to rise to a maximum of about 2400°F. The "hot" inside surface temperature was not recorded during this run.

Total Axial Strain

The total axial strain (ϵ_a) at the outside surface was measured continuously during the run and is plotted versus time in Fig. 6. The strain increases rapidly to a maximum of 7×10^3 in six seconds. This total strain includes the thermal expansion ($\alpha \Delta T$) undergone by the outside surface and therefore does not give the "effective" strain and corresponding stress which may lead to thermal shock failure.

"Effective" Axial Strain

The "effective" strain at the outside surface is obtained by subtracting the thermal expansion strain from the total strain, i.e.,

$$\epsilon_{z(\text{effective})} = \epsilon_z - \alpha \Delta T$$

where

$\epsilon_{z(\text{effective})}$ = "Effective" axial strain

ϵ_z = Total axial strain

$\alpha \Delta T$ = Thermal expansion strain at outside surface

It is the "effective" strain, rather than the total strain that produces the thermal stresses which may lead to crack initiation and fracture.

The "effective" outside surface strain is plotted versus time in Fig. 7. This "effective" strain rises steeply and almost linearly to a maximum of 2.9×10^{-3} in 3.5 seconds and then decreases more slowly with increasing time. Measurement of specimens before and after thermal shock test runs indicates that very little of the total measured strain during previous runs was due to homogeneous plastic deformation. Therefore, the "effective" strain was primarily elastic in nature. This lack of general plastic deformation increases the probability that fracture will initiate at flaws larger than some critical size. Local heterogeneous plastic strain may also occur, but is undetectable by the presently employed strain measuring technique.

Axial Stress

The outside surface stress is calculated from the following expression (see Appendix for more detailed mathematical analysis):

$$\sigma_{z(r=ro)} = \frac{E_{(r=ro)}}{(1-\mu)_{(r=ro)}} \left[\epsilon_z - (\alpha)_{(r=ro)} (\Delta T)_{(r=ro)} \right]$$

$$= \frac{E_{(r=ro)} \epsilon_{z(effective)}}{(1-\mu)_{(r=ro)}}$$

where

ro = Outside surface radius

σ_z = Axial stress

E = Elastic modulus

μ = Poisson's ratio

The axial stress versus time plot, Fig. 8, is very similar in shape to the "effective" strain curve; however, the stress contains any inaccuracy present in the elastic modulus versus temperature data employed in its calculation. Examination of existing modulus data for different types of W indicates that considerable variation exists, especially for the pressed and sintered product. The outer surface stress shown in Fig. 8 reaches a maximum value of 87,000 psi in 3-1/2 seconds at a surface temperature of 1400°F. For this particular specimen, the ductile-brittle transition temperature is not known, but it is believed that once the transition temperature is exceeded, no further crack initiation will occur. Thus, the stress required for comparison with other fracture criteria is most likely the maximum tensile stress occurring below the ductile-brittle transition temperature. Therefore, no conclusions are drawn from the comparison of the outer surface stresses with available tensile strength data.

Strain Rate

The time rate of change of total axial strain is listed in Table 1. This strain rate reaches a maximum of 4.5×10^{-3} sec^{-1} in 2.5 seconds. At the time of maximum stress, the strain rate has decreased to 1.4×10^{-3} sec^{-1}. The "effective" strain rate is approximately constant (1.7×10^{-3} sec^{-1}) almost to the time of maximum strain. At the maximum "effective" strain point, the "effective" strain rate decreases to zero and then becomes negative with increasing time. It is not known at present which strain rate, $\dot{\epsilon}_z$ or $\dot{\epsilon}_{z(effective)}$ should be compared

with the normal tensile test strain rate. It has been shown, however, that the plastic strain at fracture is highly strain rate dependent and that a strain rate of $2\text{-}5 \times 10^{-3}$ sec^{-1} can lead to an appreciable decrease in fracture ductility.[2]

Metallographic Analysis of W Specimen

A circumferential crack was found (see Fig. 9) upon sectioning and polishing the above specimen after the thermal shock test run. The crack progresses from the outside surface inward through about half the wall thickness, and does not extend around the entire circumference. It is not known for certain whether the crack occurred during the thermal shock run or later, during sectioning and mounting, but the fact that the crack is circumferential and exists only on the outer portion of the wall thickness implies that it is indeed a thermal shock crack. The voids visible along the crack length were probably caused in large part by entire grains being dislodged during metallographic polishing. This can be seen clearly in Fig. 10, where the large void has a characteristic grain shape. It is also obvious from this figure that the crack is predominantly intergranular in nature. Examination of Fig. 9 discloses what appear to be several almost parallel crack branches; however, it is possible that some of these are independently initiated cracks. Due to the relatively low maximum temperature and short time of the test run, one would not expect to find any rounding off of the sharp edges and of corners at crack bends, and this appears to be the actual case.

The correlation of maximum "effective" strain or fracture stress with the fracture strain and stress as determined in tension is being investigated. Because property data for W is so sensitive to prior history and type, it is planned in the future to make duplicate cylindrical specimens; one will be used in a thermal shock run, and the others will be tested for fracture stress, fracture strain, ductile-brittle transition temperature, and strain rate sensitivity. Excellent tests are available for determining these properties using a hollow cylindrical test specimen.[3]

A comparison of the thermal stress and strain data determined experimentally in this study with the data calculated from theoretical considerations by Vigness and Clements[4] for the case of a flat plate subjected to a similar temperature rise shows considerable agreement. In both cases, the thermal stress and "effective" strain rise rapidly to a maximum in the first several seconds and then fall off somewhat more gradually. It is planned to investigate more thoroughly the correlation between experimentally determined and theoretically predicted stress and strain behavior for the case of a hollow cylinder.

Conclusions

It may be concluded from the above discussion and analysis that the presently developed thermal shock investigative procedure will provide valuable data in elucidating the following effects:

1. Effect of wall thickness and O. D. /I. D. ratio on the thermally induced stresses and strains produced on the outer surface of hollow tungsten cylinders subjected to rapid heating conditions from the inside surface.

2. Effect of type of tungsten, e. g., copper or silver-infiltrated tungsten, on the magnitude of thermally induced stresses and strains. It may be possible, for instance, that any increased thermal conductivity of an infiltrated material will lead to lower outside surface stresses.

3. Effect of type of tungsten on the tendency to undergo thermal shock cracking at a given stress or strain level. This study could lead to the establishment of a materials thermal shock parameter for tungsten.

Effects 1 and 2 may be analyzed with a fair degree of accuracy using data obtainable with the thermal shock apparatus. Effect 3, however, will require additional knowledge of actual mechanical properties as a function of temperature for each type of tungsten investigated.

Future Work

Erosion Study

The effect of temperature and CO_2 flow rate on the erosion of coarse grain, pressed, sintered, and swaged tungsten will be determined. Other exhaust constituents and other types of tungsten will also be investigated.

Thermal Shock Study

It is planned to investigate the effect of wall thickness, density, and type of tungsten on thermal shock resistance.

It is also planned to have the fracture stress, fracture strain, and ductile-brittle transition temperature determined for a series of tungsten cylinders of varying densities and types. Duplicates of each of these cylinders will then be tested in the thermal shock apparatus and an attempt will be made to correlate material properties with thermal shock resistance.

Work will also continue on a mathematical analysis and correlation of theoretically predicted and experimentally determined stress and strain data.

Gerald M. Gordon
Senior Metallurgist

David A. Brown
Metallurgist

GMG:DAB/emk
Approved:

A. E. Gorum, Director
Material Sciences Division

Appendix

THERMAL STRESS BEHAVIOR IN A CONCENTRICALLY HEATED HOLLOW CYLINDER

In the succeeding calculations, the following assumptions are made.

1. The temperature distribution and corresponding strains at any time are assumed to be symmetrical about the cylindrical axis and constant along this axis.

2. The cylinder is unrestrained by external forces.

3. The axial strain is constant across the entire wall thickness. This statement is strictly valid only for strains distant from the cylinder ends and thus a sufficiently long cylinder is assumed.

4. The cylinder is isotropic, perfectly elastic, and homogeneous.

Consider a section perpendicular to the cylindrical axis z and distant from the cylinder ends

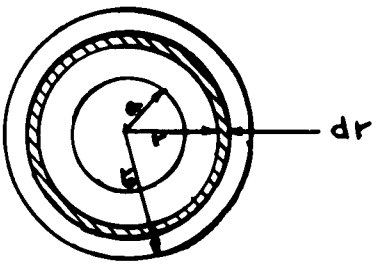

From equilibrium considerations, it can be shown[5] that the axial stress acting on a cylindrical element of thickness, dr, sufficiently small so that the temperature does not vary across it, is given by the following expression

$$\sigma_{z(r)} = \frac{E_{(r)}}{(1-\mu)_{(r)}} \left[\epsilon_z - (\alpha)_{(r)}(\Delta T)_{(r)} \right] \qquad (A-1)$$

where

σ_z = Axial stress

E = Elastic modulus

μ = Poisson's ratio

ϵ_z = Axial strain

$\alpha \Delta T$ = Potential thermal expansion strain

It can also be shown that the other stresses acting on the increment are related to σ_z by the following:

$$\sigma_{z(r)} = \sigma_{\theta(r)} + \sigma_{r(r)} \tag{A-2}$$

where

σ_θ = Circumferential stress

σ_r = Radial stress

At the cylindrical surfaces, σ_r is obviously zero and therefore

$$\sigma_{z(r=a)} = \sigma_{\theta(r=a)} \tag{A-3}$$

$$\sigma_{z(r=r_o)} = \sigma_{\theta(r=r_o)} \tag{A-4}$$

At equilibrium, summing forces in the z direction gives

$$2\pi \int_{r=a}^{r=b} \sigma_{z(r)}\, r\, dr = 0 \tag{A-5}$$

Substitution of (A-1) into (A-5) gives

$$2\pi \int_{r=a}^{r=r_o} \frac{E_{(r)}}{(1-\mu)_{(r)}} \left[\epsilon_z - (\alpha)_{(r)} (\Delta T)_{(r)}\right] r\, dr = 0 \tag{A-6}$$

Solving for ϵ_z gives

$$\epsilon_z = \frac{\int_{r=a}^{r=r_o} \frac{E_{(r)}}{(1-\mu)_{(r)}} (\alpha)_{(r)} (\Delta T)_{(r)}\, r\, dr}{\int_{r=a}^{r=r_o} \frac{E_{(r)}}{(1-\mu)_{(r)}}\, r\, dr} \tag{A-7}$$

Equation (A-7) is general and takes into account any variations in physical properties with temperature.

In this study, thermal stresses are calculated directly from equation (A-1) since the axial strain is measured during each test run. If we assume that $\mu \neq (T)$, then it is obvious from equation (A-1) that the maximum axial stress (and also circumferential stress) occurring during rapid heating of the inside surface will exist at the "cold" outside surface (r=ro) where $\alpha \Delta T$ is a minimum and elastic modulus is a maximum. During heating, this stress is tensile in nature and if sufficiently large it can lead to crack initiation and propagation in a "brittle" material.

Where this strain cannot be measured due to experimental difficulties (e.g., in an actual rocket firing), it is necessary to calculate it from equation (A-7). An exact solution of equation (A-7) for axial strain cannot however, be made, in general, and it is therefore necessary to use approximation methods such as employed by Vigness and Clements[4] for the case of a flat plate.

REFERENCES

1. Progress Report No. 19, February 1, 1962.

2. J. H. Bechtold, "Strain Rate Effects in Tungsten," AIME Transactions, 206, 142-146 (1956).

3. S. A. Bortz and H. H. Lund, "Evaluation of a Tension Test for Brittle Materials," Proceedings of the Fourth Conference on Carbon, Pergamon Press, New York and London (1960), p. 531.

4. I. Vigness and E. W. Clements, "Thermal Stress Transients in a Flat Slab," NRL Project 62RO5-19B, Tech. Memo. No. 179, Shock and Vibration Folder No. 908, November 30, 1961.

5. S. Timoshenko, "Theory of Elasticity," McGraw-Hill Book Co., Inc., New York and London, 2nd Edition (1951), p. 408-413.

Table I*

MECHANICAL AND THERMAL DATA FOR A 94% DENSE TUNGSTEN SPECIMEN

TIME (sec)	$T(r = r_0)$ (°F)	$\epsilon_z(r = r_0)$	$(\alpha\Delta T)^{\dagger}(r = r_0)$	$(\epsilon_z - \alpha\Delta T)(r = r_0)$	$E^{\dagger}(r = r_0)$ (psi)	STRAIN RATE $\dot{\epsilon}(r = r_0)$ (sec^{-1})	$\sigma_z(r = r_0)$ (KSI)	TENSILE STRENGTH (KSI)
0	70	0	0		42×10^6	0	0	36
1.0	105	~ 0	0.08×10^{-3}	~ 0	41×10^6	~ 0	~ 0	36
1.5	175	0.2×10^{-3}	0.26×10^{-3}	~ 0	39.5×10^6	1.2×10^{-3}	~ 0	36.5
2.0	375	1.5×10^{-3}	0.8×10^{-3}	0.7×10^{-3}	35×10^6	2.9×10^{-3}	35	37.5
2.5	787	3.3×10^{-3}	1.8×10^{-3}	1.5×10^{-3}	26.5×10^6	4.5×10^{-3}	57	39
3.0	1115	5.1×10^{-3}	2.6×10^{-3}	2.5×10^{-3}	21.5×10^6	2.4×10^{-3}	77	39
3.5	1400	6.2×10^{-3}	3.3×10^{-3}	2.9×10^{-3}	21×10^6	1.4×10^{-3}	87	38
4.5	1840	6.8×10^{-3}	4.4×10^{-3}	2.4×10^{-3}	21×10^6	3.5×10^{-4}	72	36
6.5	2240	7.1×10^{-3}	5.4×10^{-3}	1.7×10^{-3}	20.5×10^6	0	49	30

* All terms used are defined in Appendix.

† α, E, and tensile strength taken from data supplied by Aerojet General Corporation for 95% dense pressed and sintered tungsten.

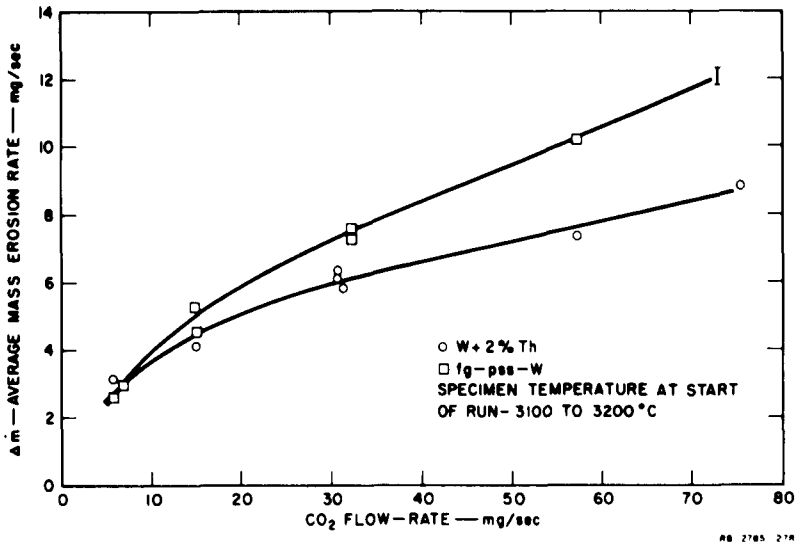

FIG. 1 AVERAGE W-EROSION RATE vs. CO_2 - FLOW RATE

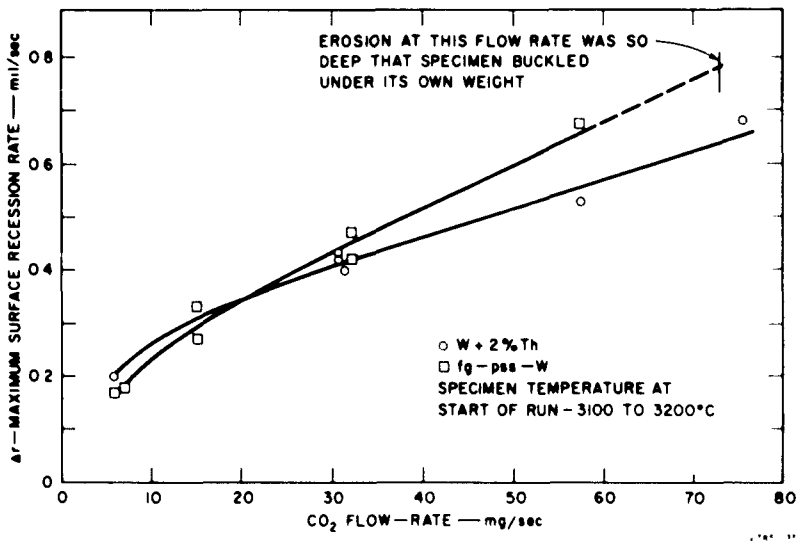

FIG. 2 MAXIMUM SURFACE RECESSION RATE vs. CO_2 - FLOW RATE

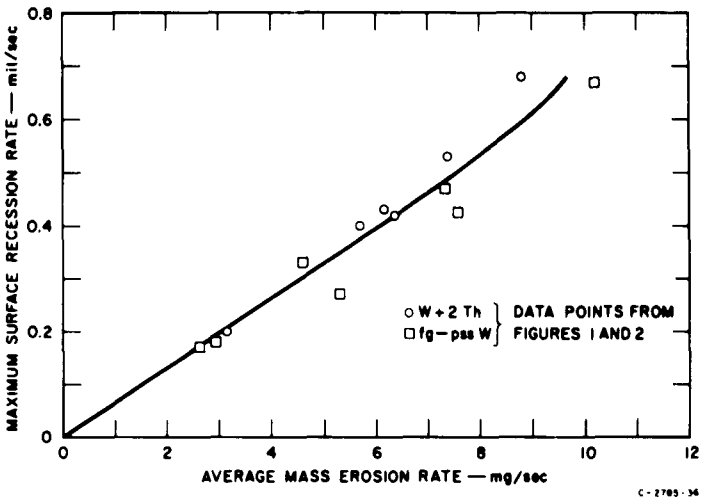

FIG. 3 MAXIMUM SURFACE RECESSION RATE vs. MASS EROSION RATE

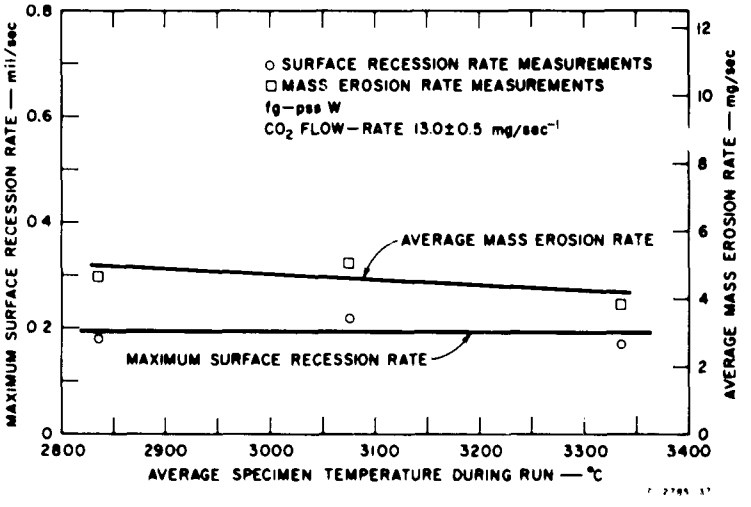

FIG. 4 EROSION RATE OF fg-pss W vs. TEMPERATURE

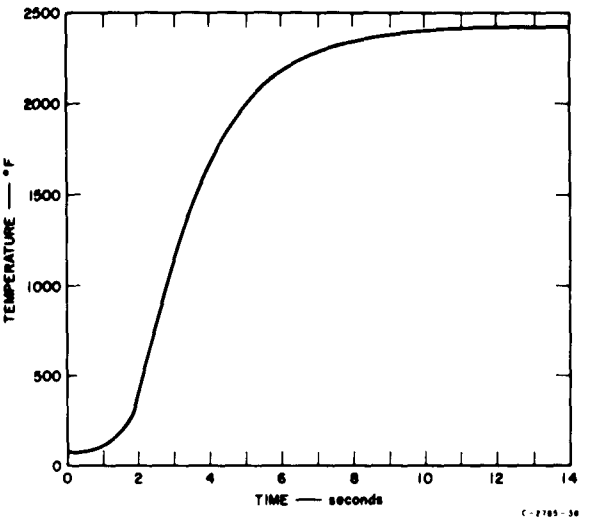

FIG. 5 TEMPERATURE RATE ON THE OUTSIDE SURFACE OF A 1.14" I.D. × 1.54" O.D. × 0.75" HIGH, 94% DENSE, PRESSED AND SINTERED W CYLINDER

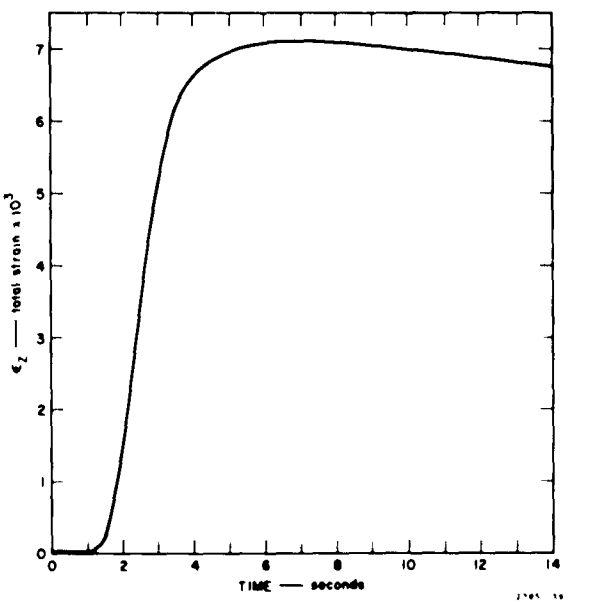

FIG 6 MEASURED TOTAL AXIAL STRAIN (ϵ_z) vs. TIME PLOT FOR W CYLINDER

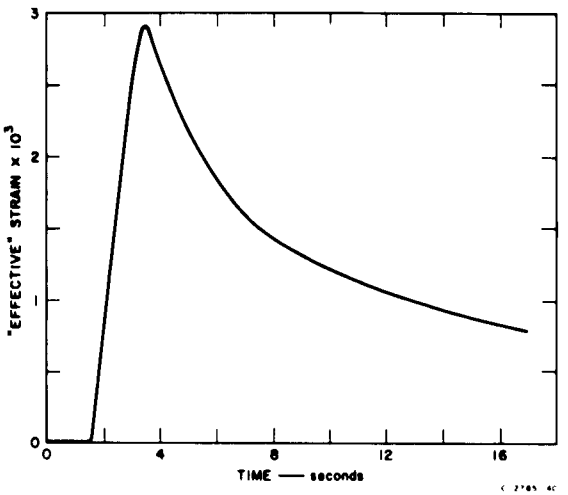

FIG. 7 "EFFECTIVE" AXIAL STRAIN ($\epsilon z - \alpha\Delta T$) vs. TIME PLOT FOR THE OUTSIDE "COLD" SURFACE

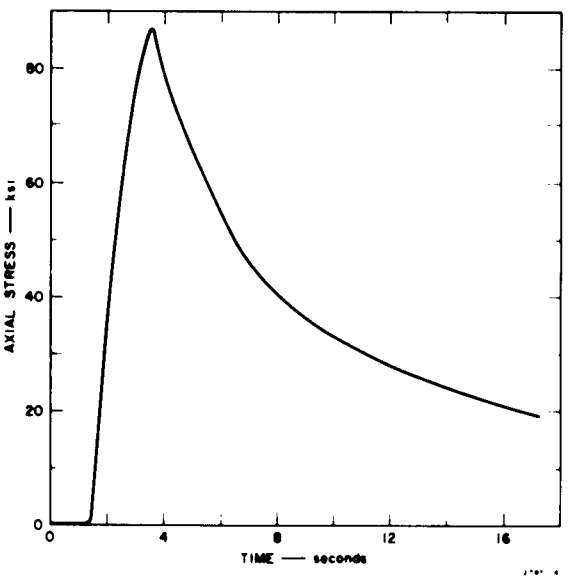

FIG. 8 AXIAL STRESS AT OUTSIDE SURFACE OF W CYLINDER vs. TIME

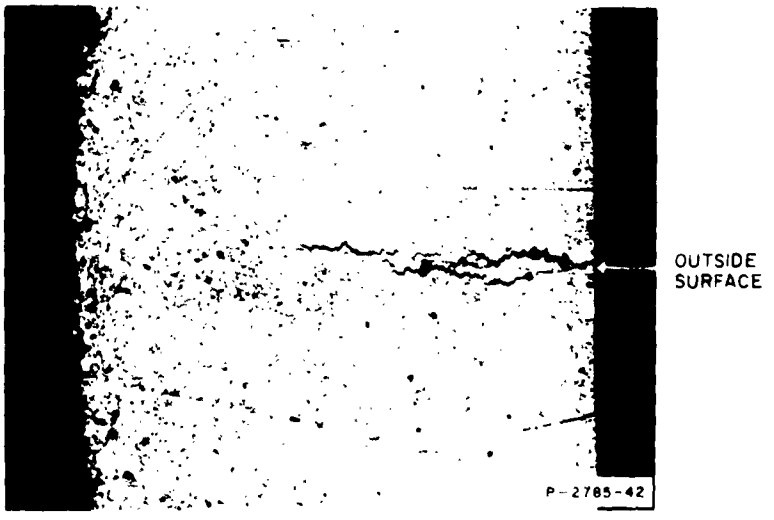

FIG. 9 CIRCUMFERENTIAL CRACKS PRODUCED DURING THERMAL SHOCK TEST RUN ON 94% DENSE HOLLOW TUNGSTEN CYLINDER (20X)

FIG. 10 SECTION OF CIRCUMFERENTIAL CRACK PRODUCED DURING THERMAL SHOCK TEST RUN (500X)